Microporous and Mesoporous Materials 190 (2014) 362–370

Contents lists available at ScienceDirect

Microporous and Mesoporous Materials

journal homepage: www.elsevier.com/locate/micromeso

Influence of porous substrate on copper based oxygen carrier efficiency for chemical-looping combustion

Noemie van Garderen [a,b,*], Eugenio H. Otal [c,d], Christos G. Aneziris [b], Thomas Graule [a,b], Frank J. Clemens [a,*]

[a] Empa, Swiss Federal Laboratories for Materials Science and Technology, Laboratory for High Performance Ceramics, Ueberlandstrasse 129, 8600 Dübendorf, Switzerland
[b] Technical University Bergakademie Freiberg, Institute for Ceramic, Glass- and Construction Materials, Agricolastraße 17, 09596 Freiberg, Germany
[c] Empa, Swiss Federal Laboratories for Materials Science and Technology, Solid State Chemistry and Catalysis, Ueberlandstrasse 129, 8600 Dübendorf, Switzerland
[d] UTN – Santa Cruz Regional Faculty, Río Gallegos, Santa Cruz, Argentina

ARTICLE INFO

Article history:
Received 24 October 2013
Received in revised form 4 February 2014
Accepted 6 February 2014
Available online 15 February 2014

Keywords:
Oxygen carrier support
Microstructure
Looping efficiency
Attrition resistance

ABSTRACT

The efficiency of impregnated redox material and its cycling behaviour by tailoring macro- to mesoporosity of different support compositions for fluidized-bed application was investigated. Supports are composed of clay and diatomite, alumina, alumina and diatomite, alumina diatomite and silica. The porous supports were impregnated with 1.5 M copper nitrate trihydrate and calcined at 850 °C. Higher presence of copper has been determined on samples composed of higher specific surface area and larger pore size distribution. Presence of CuO and Cu_2O phases were obtained in silica based samples (clay, diatomite or silica nanoparticles), whereas $CuAl_2O_4$ dominated in samples with high alumina content. Reaction rate-during reduction increased with silica, while total conversion was reduced. Highest conversion was obtained for alumina samples because of the aggregation of copper on pure silica surfaces. It is assumed that after infiltration of 10 wt.% copper phase, surface chemistry is of great importance compared to pore size. Wet impregnation had no effect on attrition resistance.

1. Introduction

Chemical-looping combustion CLC is considered as one of the most promising technique for CO_2 separation of fossil fuel combustion. It is considered as a form of oxy-fuel combustion because it does not involve nitrogen in the fuel reactor, leading to the elimination of NO_x emissions. Fan categorized CLC as a pre-combustion and oxy-combustion capture technique because of the removal of carbon present in the fuel before combustion and because of the use of an oxygen carrier (e.g. pure oxygen) instead of air [1]. CLC is based on the idea developed by Lewis and Gilliland [2] on producing pure CO_2 from fossil fuels with two fluidized bed reactors. CLC involves the use of an oxygen carrier (metal oxide), which transfers oxygen from an air reactor to a fuel reactor for combustion, without direct contact between fuel and air (Fig.1). Fuel and metal oxide Me_xO_y (oxygen carrier) react in a fuel reactor composed of gases, such as CH_4, CO and H_2, or solid fuel, such as biomass or coal [3]. The almost pure stream of CO_2 can be separated for CO_2 storage by water condensation with a small loss of energy. In the fuel reactor, the metal oxide will be reduced into Me_xO_{y-1}, which is either endothermic or exothermic, depending on the types of oxygen carrier and fuel used in the reaction. After almost complete conversion, the obtained reduced metal oxide is transferred to an air reactor (high-velocity riser [4], where the volumetric flow rate is about ten times higher than in the fuel reactor) to be reoxidized according to the exothermic process (1).

$$Me_xO_{y-1} + 1/2\,O_2 \rightarrow Me_xO_y \quad (1)$$

By thermogravimetric analyses, de Diego et al. found out that CuO without support lost 90% of its initial reactivity after only three cycles of reduction and oxidation, while no loss could be observed with the use of a silica support [5]. Several properties are required for the oxygen carrier, such as: high redox activity during oxidation and reduction, good oxygen transport capacity, negligible carbon deposition, high attrition resistance, low tendency for agglomeration during the use in a fluidized bed reactor, to be environmental friendly and economic. The porous support material has to be moreover composed of: highly interconnected open porosity to facilitate the oxygen carrier impregnation, high specific surface

* Corresponding authors at: Empa, Swiss Federal Laboratories for Materials Science and Technology, Laboratory for High Performance Ceramics, Ueberlandstrasse 129, 8600 Dübendorf, Switzerland. Tel.: +41 58 765 48 21; fax: +41 58 765 41 50.

E-mail addresses: vangarderennoemie@yahoo.fr (N. van Garderen), frank.clemens@empa.ch (F.J. Clemens).

http://dx.doi.org/10.1016/j.micromeso.2014.02.017
1387-1811/

area, low neck and ink-bottle contents to optimise the exchange of oxygen gas and high attrition resistance to withstand the mechanical and chemical stresses during its use in a fluidized bed reactor.

Abad et al. reported a mapping of different metal oxides, their advantages and drawbacks with the range of temperature they can be used [6]. The reactivity of the oxygen carriers is frequently classified in descending order, as the following: NiO, CuO, Fe_2O_3 and Mn_2O_3 [7]. In addition, Cole patented some oxides of silver, tungsten and molybdenum as well as sulphates of barium and strontium as potential oxygen carriers [8]. However, only oxygen carriers based on Cu, Fe and Mn show a complete fuel gas conversion [9]. Adanez et al. succeeded to use a mixture of CuO and NiO as oxygen carriers [10]. CuO leads to a complete conversion of CH_4 to CO_2 and H_2O and the use of NiO permits to increase the temperature up to 950 °C [10].

Materials such as SiO_2, TiO_2, ZrO_2, Al_2O_3, YSZ have been frequently used so far as oxygen carrier support, but study on the influence of the porous support structure on the performance of oxygen carriers has not been done so far. Jerndal et al. mentioned the importance of melting temperature, heat balances of the fuel reactions in case of endothermic reactions in the fuel reactor, carbon or sulphur reactions that might be produced in the fuel reactor [9].

The bed materials developed in this work aim to be used in a CLC process adapted to a 10 kW_{SNG} scale reactor for wood methanation, which was built by Paul Scherrer Institute and transferred to the gasifier in Güssing, Austria [11]. The copper loading and the looping efficiency of granulates based on clay/diatomite (Route 1), alumina (Route 2), alumina/diatomite (Route 3-a), and alumina/diatomite/silica (Route 3-b) were analysed in function of the phase composition and microstructure (from macro- to mesopores range). Moreover, the attrition resistances before and after impregnation, as well as after looping efficiency were performed on two selected samples.

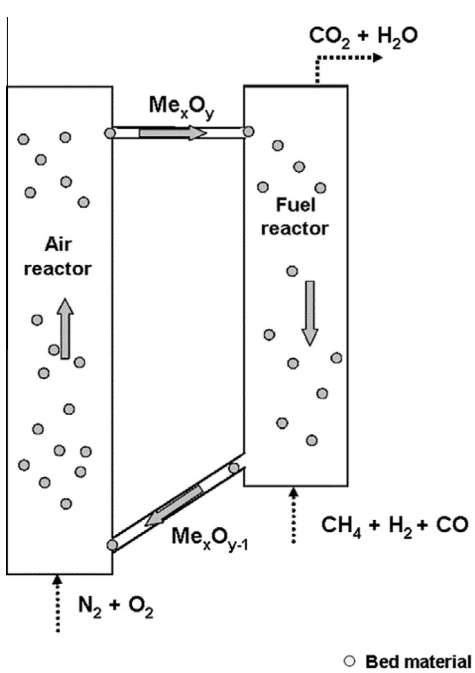

Fig. 1. Schematic principle of CLC fluidized bed reactor.

2. Experimental procedure

2.1. Raw material

Different raw materials were investigated to determine the influence of the chemical surface and microstructure on the performance of the developed bed materials. Fig. 2 shows an overview of the different raw materials and their processing routes to achieve the porous granulates.

Except in the case of Route 2, two diatomite filter aids Filter Cel and Super Cel (Celite, World Minerals Inc., USA) with specific surface areas of 8.8 and 2.7 m^2/g, median particle sizes of 14 and 15 μm and a median pore size of 2.5 and 3.5 μm (supplier data) were used to achieve a highly porous structure after heat treatment. Both diatomites are composed of approximately 90% of SiO_2 and 4% of Al_2O_3.

For the Route 1, 48 vol.% of clay kaolin EKA-S (Amberger Kaolinwerke, Germany) was used as a plasticiser and inorganic binder to bridge the diatomite particles after thermal treatment. EKA-S is composed mainly of 55% kaolinite, 24% illite and montmorillonite and 20% quartz.

Pseudo-boehmite G-250 (BASF, USA) with an agglomerate size d_{50} of 60 μm (given by the supplier), based on conversion of bauxite into gibbsite by the Bayer process, followed by an acid/base dissolution and precipitation, was selected for Routes 2 and 3.

Silica dispersion Levasil 50/50 (Obermeier, Germany) with a specific surface area of 50 m^2/g was used in a mixture of alumina and diatomites to tailor the porosity and the specific surface area of the granulates (Route 3-b).

For the wet impregnation step, copper nitrate trihydrate from Sigma–Aldrich (61194, Switzerland) was selected due to its high purity (>99%).

2.2. Granulate production

2.2.1. Route 1_clay/diatomite based samples

Dry powders were premixed for 3 min in a planetary mixer before adding an emulsion of deionised water and oil. After approximately 6 min of mixing time, the feedstocks were shaped with a piston extruder (Type 232 16 DT-HS, Loomis, Germany) at a pressure of 40–50 bar through a die with an orifice of 500 μm. The extruded materials were dried for 3 days at 60 °C before being ground and sieved into granulates with a size from 180 to 500 μm. Finally, granulates were sintered in air at 1100 °C for 3 h in a furnace (PY 12H, Pyrotec) with a heating rate of 110 °C/h. Processing was detailed previously [12,13].

2.2.2. Route 2_alumina samples

Samples were prepared with a constant solid content of 82 wt.% and peptized with 1.87 M acetic acid [GAR12]. After 60 min kneading time at 40 rpm (Janke and Kunkel, IKA Labortechnik RE 162/P Analog, Germany), the ceramic feedstocks were shaped into cylindrical extrudates (ϕ = 1.5 mm) using a capillary rheometer (Rosand RH7, Malvern, Germany) and dried for 48 h at room temperature. In order to obtain the γ-alumina phase, the extrudates were calcined in air at 5 °C/min until 850 °C with a dwell time of 120 min. Granulates with a size between 180 and 500 μm were finally obtained by grinding and sieving. Processing and characterization was previously reported [14].

2.2.3. Route 3-a_alumina/diatomite based samples

Pseudo-boehmite and diatomites were first mixed for 2 min at 25 rpm, the acetic acid solution was then added to the solid materials and after the third minute, the speed was increased to 30 and 40 rpm after the fourth minute. After 6 min kneading, the organic

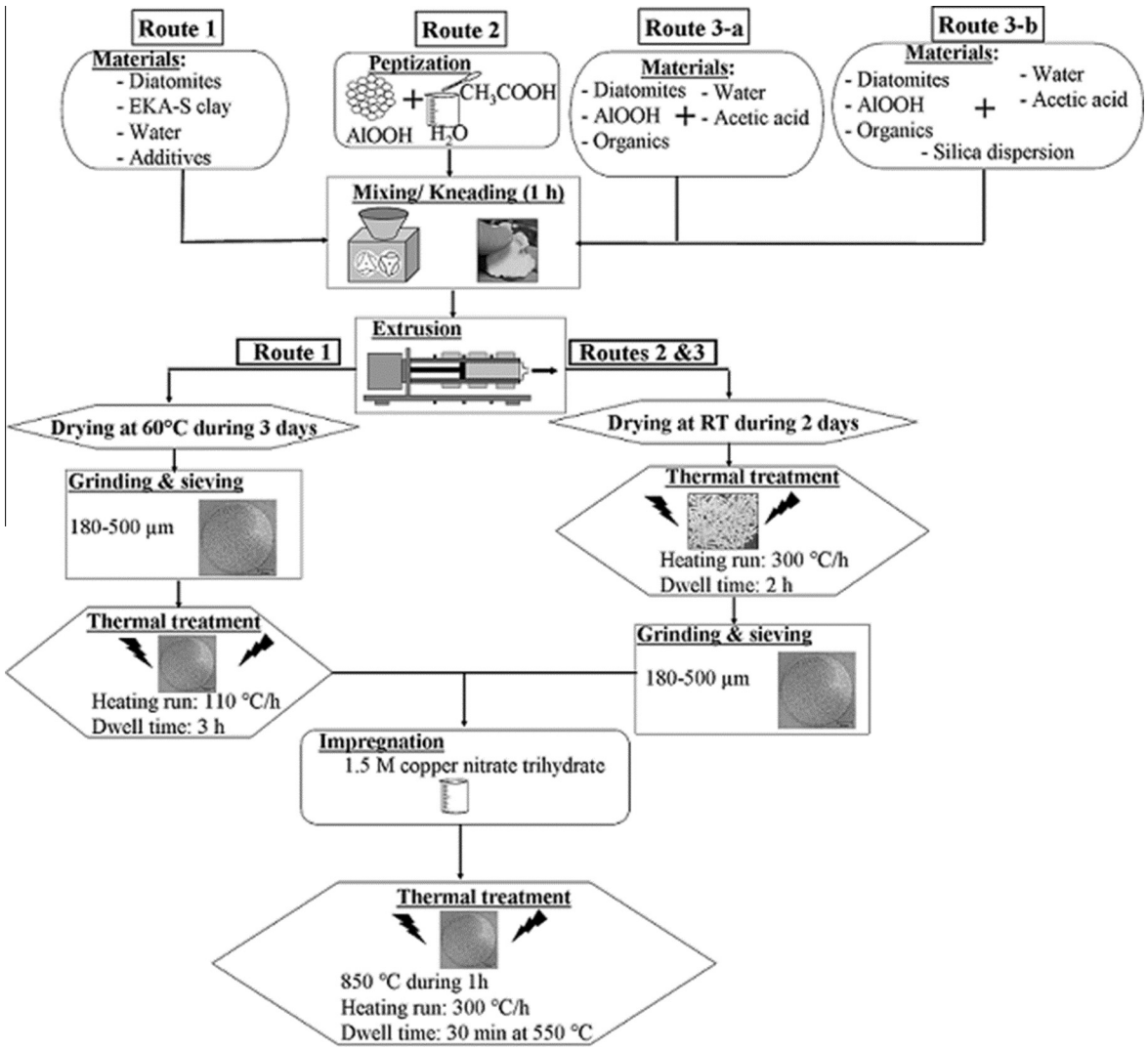

Fig. 2. Schematic processing routes for the different extruded porous substrates.

binders were added. Total compounding step took 1 h. The feedstock was afterwards extruded through a 1.5 mm diameter die into a capillary rheometer (Rosand RH7, Malvern, Germany) and dried for more than 48 h at room temperature. The calcination step was carried out in air at 5 °C/min to 850 °C with a dwell time of 2 h. Granulates with a size between 180 and 500 µm were prepared by grinding and sieving after heat treatment. More details can be found elsewhere [15].

2.2.4. Route 3-b_alumina/diatomite/silica based samples

34 vol.% silica dispersion Levasil 50/50 (Obermeier, Germany) was added after 6 min kneading to the pseudo-boehmite and diatomites compound. The feedstocks were extruded through a 1.5 mm diameter die with a capillary rheometer (Rosand RH7, Malvern, Germany) and dried for more than 48 h at room temperature. The calcination was performed in air at 5 °C/min to 850 °C with a dwell time of 2 h. More information was already reported [15].

2.2.5. Impregnation

Granulates were wet impregnated for 14 h in a 1.5 M copper nitrate trihydrate solution. The liquid- to granulates ratio was fixed to 12.5 mL.g^{-1}. The material was then filtered to remove the excess of solution and dried at 80 °C during 24 h. The impregnated granulates were calcined at 550 °C for 30 min in order to decompose it into copper oxide, as described by Forero et al. [4]. A thermal treatment at 850 °C for 1 h in air was followed to stabilize the oxygen carrier.

2.3. Characterization

2.3.1. Microstructure investigations

Total porosity and median pore size were evaluated with a mercury porosimeter MP (Pascal 140/440, Thermo Fisher, Germany). Surface tension and contact angle of mercury were set to 0.480 N/m and 140°, respectively. Mesoporosity was evaluated with nitrogen sorption at 77.4 K with a BET device (type SA 3100, Coulter, Switzerland), using Barrett–Joyner–Halenda (BJH) model based on the Kelvin–Laplace equation [15] from the nitrogen desorption plot. Pore shape was determined from the hysteresis according to IUPAC classification. Samples for both measurements were dried 14 h at 180 °C in order to drive off any physisorbed water from the sample.

Scanning electron microscopy (SEM) with a back-scattered detector was performed with a TS 5136MM apparatus (Tescan, Germany) to investigate the sample microstructure on cross-sections after impregnation and looping steps.

Scanning electron microscopy with Energy-Dispersive X-ray Spectrometry (SEM–EDX) was performed with a TEM Grid (Plano

GmbH, Germany) to determine the presence of copper on some selected impregnated samples.

2.3.2. Phase structure

For the chemical phase analysis, an X-ray powder diffractometer X'Pert Pro PW3040 (PANanalytical, Switzerland) with Cu target (Kα, $\lambda = 0.15406$ nm) with radiation at 45 kV and 40 mA settings was used.

2.3.3. Looping efficiency

The mass spectroscopy was performed on three selected samples to investigate the effect of macro- to mesoporosity. The looping experiments were made in a Netzsch STA 409 CD thermobalance coupled to a Netzsch QMS 403 C Aeolos mass spectrometer. The following gases were used: 10% CO (purity ± 2%) and 90% He were selected as the reducing fuel and synthetic air (20% O_2 (purity ± 1% O_2) and 80% N_2) as the oxidizing gas). At 850 °C, the oxidizing and reducing gases were interchanged every 20 min to stabilize the oxidized or reduced carrier. Between each gas, nitrogen was flushed during 5 min to clean the chamber. To investigate oxidation of CO at 850 °C, 150 mg granulates were used in alumina crucibles and a CO gas flow rate of 50 ml/min. The looping efficiency E corresponds to the maximum weight change during reduction step and is calculated with Eq. (2). Conversion rate corresponds to the slope of reduction and oxidation line.

$$E = (m_{ox} - mr_{ed})/m_{ox} * 100 \quad (2)$$

2.3.4. Attrition resistance analysis

An easy and reproducible grinding test was developed to determine the mechanical resistance of granulates with a size between 180 and 500 μm. Attrition tests were performed on a roller mixer (type RM1, Zoz GmbH) and experiments were performed with 4 zirconium oxide balls (25 mm in diameter) in a standard 250 ml polyethylene bottle. The rotation speed was fixed to 60 rpm and 2 g of material were used. Determinations of the attrition resistance as well as the use of the attrition resistance index as a comparison technique were reported previously [12].

3. Results and discussion

3.1. Impregnation

Content of oxygen carrier is frequently about 10–30 wt.% by using impregnation method [16]. Chuang et al. succeeded to increase CuO loading to 82.5 wt.% by co-precipitation technique, it is highly pH dependant [17]. Adanez et al. however mentioned the necessity to have a CuO content lower than 20 wt.% in order to avoid agglomeration effect during fluidization process [17]. In this study we focused on impregnation method to achieve similar Cu content, which is necessary to investigate the influence of pore structure and phase composition. As explained by Fan, it is difficult to determine the metal loading after impregnation because of the inherent nature of the technique [1]. Copper oxide can indeed react with the substrate material, especially alumina and form new phases of different densities. Therefore the metal loading in this work was calculated based on the weight gain of the copper nitrate impregnated granulates, after drying over night at 80 °C and the molar weight of the copper in the copper nitrate salt. Fig. 3 shows the presence of copper on samples composed of different microstructure. As seen in Fig. 3, the highest copper impregnation was observed in sample from Route 2, which was composed of a high specific surface area, smallest pore size distribution and high pore volume (see Section 3.2). For granulates with lower specific surface areas, the increase in mean pore sizes allowed the impregnation of higher copper content due to infiltration of the solution into the interconnected open porous granulates.

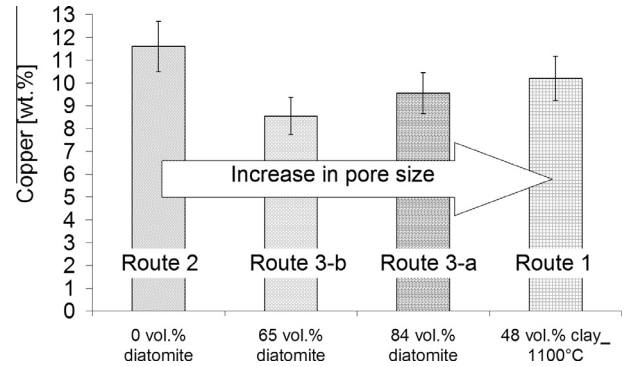

Fig. 3. Metal loading impregnated on the different porous supports.

3.2. Microstructure

Mercury porosimetry results of the four granulates are shown in Fig. 4. For better comparison reason, the pore volume of the samples was normalized. A detailed description of the clay based granulates (Route 1) can be found elsewhere [12,13]. By addition of 84 vol.% diatomite, the pore size distribution of the granulates can be tailored from meso- to macroporosity, see Route 2 and Route 3-a in Fig. 4a and b. Samples from Route 2 (γ-Al_2O_3 with 0 vol.% diatomite) and from Route 3-b (γ-Al_2O_3 with 65 vol.% diatomite and 34 vol.% silica) show an increase in mesoporosity after impregnation. This can be explained by formation of copper agglomerates, which forms an interparticular porosity. More pronounced change in pore size distribution was observed by samples only composed of alumina because in this material almost pure mesoporosity is present (Fig. 4a). Concerning samples from Route 1 (diatomite-clay based samples, Fig. 4a) and from Route 3-a (with 84 vol.% diatomite, Fig. 4b), a slight decrease in the macropores size is observed because of the presence of copper phase in the larger pores. This confirms good impregnation of pores in the micrometer range.

Influences of impregnation on porosity and median pore size are shown in Table 1. A decrease in porosity was observed. For few samples, the median pore size was similar or slightly increased after impregnation. Mesoporous material (samples from Route 2 – γ-Al_2O_3 material granulates) showed a decrease in porosity of about 11%, while a decrease of more than 45% was observed on sample composed of meso- and macroporosities (Route 3-a). 20% decrease in porosity was determined on samples from Route 1 (clay-diatomite granulates). The slight increase in porosity for samples from Route 3-b, can be explained by the formation of copper oxide agglomerates, which formed interparticular porosity in the mesopore range.

Samples with pores in the macro-range showed a decrease in median pore sizes after impregnation, while samples with mesopores were composed of larger pore sizes after the impregnation step. The mesopore size distribution of the copper oxide particle (e.g. agglomeration) was indeed higher in comparison to the substrate, the increase in median pore sizes can thus be explained. Especially supports with dominated meso-porous structure, e.g. high alumina or/and Levasil content lead to higher porosity and median pore sizes, while specific volume decreased, as expected, after impregnation (Table 1).

In Fig. 5, the pore volumes before and after impregnation are shown. The results confirm the significant influence of macropores compared to mesopores during the impregnation step. For example, samples from Route 3-b, composed of both meso- and macropores, showed a higher decrease in the pore volume

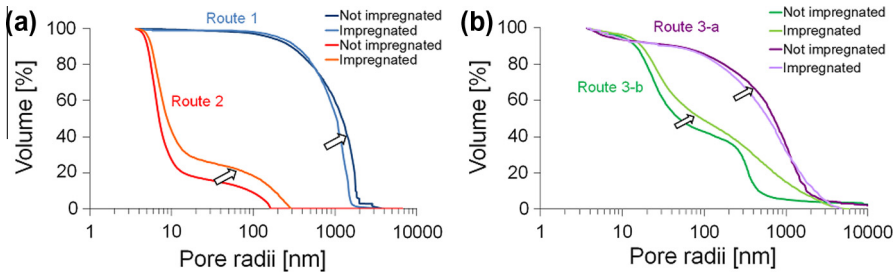

Fig. 4. Mercury porosimetry of granulates before and after impregnation, (a) Route 1: clay based diatomite material, Route 2: γ-alumina, (b) Route 3-a: γ-alumina sample with 84 vol.% diatomite, Route 3-b: γ-alumina sample with 65 vol.% diatomite and 34 vol.% silica.

Table 1
Porosity and median pore radius determined by mercury porosimetry analyses of the developed products before and after impregnation.

	Porosity [%]		Median pore radius [nm]	
	Not impregnated	Impregnated	Not impregnated	Impregnated
48 vol.% clay_1100 °C Route 1	68	54	1201	1048
0 vol.% diatomite Route 2	61	54	4	11
84 vol.% diatomite Route 3-a	71	38	717	609
65 vol.% diatomite Route 3-b	28	37	49	93

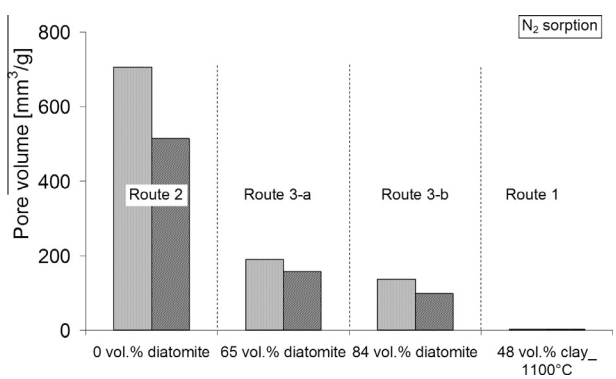

Fig. 5. Variation of pore volume determined by nitrogen sorption before (light grey) and after (dark grey) impregnation.

determined from MP (e.g. macroporosity). This confirms that copper oxide is infiltrated into a large porous network, while it has the tendency to cover the surface of granulates composed of smaller pores.

Table 2 summarizes the results of nitrogen sorption analyses of the samples before and after impregnation and also after CLC tests. No tests were performed by MP because of the too small sample size used for CLC tests. As expected, a decrease in specific surface area occurred after sample impregnation, as well as after looping experiments. This permits to conclude to the blocking of smaller pores observed after impregnation and the coalescence of the structure after further thermal treatment.

The use of diatomite and silica resulted in a decrease in specific surface area. Lower volumes were moreover observed by addition of diatomite and silica, because of the small mesopores volume in diatomite filer aids [18,19] and the blocking of small pores with silica nanoparticles.

3.3. Looping experiments

During the looping experiments in a TGA device, reducing and oxidizing gases were interchanged to achieve decrease and increase in mass loss of the oxygen carrier, respectively. As seen in Fig. 6, a higher mass change was obtained with sample from Route 2. Samples from Route 1 and Route 3-b showed similar behaviour after few hours test. However, sample from Route 1 showed a shift in the mass variation. No complete oxidation can be reached after less than 10 h measurements.

In order to evaluate the efficiency of the bed material, the presence of copper impregnated in the carrier was compared to the one, which reacted during looping tests in a thermogravimetric machine. It was found out that 58 ± 6% of copper reacted for clay based granulates (Route 1), while 72 ± 7% reacted for alumina samples (Route 2) and for diatomite-silica ones (Route 3-b). Higher

Table 2
Specific surface areas and specific volumes of the developed samples, before, after impregnation and after CLC cycling.

	Specific surface area [m^2/g]			Specific mesopore volume [mm^3/g]		
	Not impregnated	Impregnated	After CLC cycling	Not impregnated	Impregnated	After CLC cycling
Route 1						
48 vol.% clay_1100 °C	2	1	–	4	4	–
Route 2						
0 vol.% diatomite	153	105	57	706	515	403
Route 3-a						
84 vol.% diatomite	36	17	5	138	99	80
Route 3-b (34 vol.% silica)						
65 vol.% diatomite	17	15	11	190	157	160

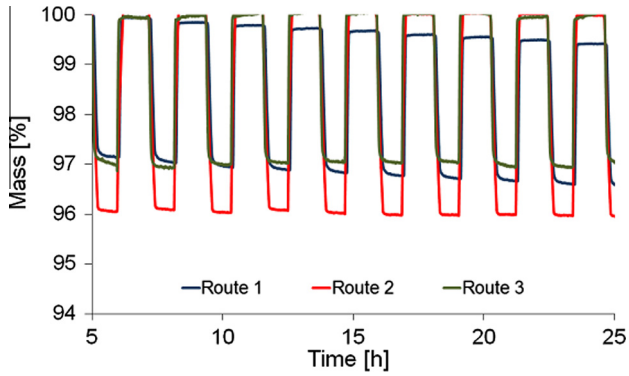

Fig. 6. Mass change during reducing and oxidizing reactions.

reactivity for the alumina and diatomite-silica granulates was expected because of the presence of oxygen carrier on the surface of the granulates with smaller pores. Therefore it can be assumed additionally to the wet impregnation that wet bulk deposition [20] occurs in this study for granulates with small pores. The efficiency obtained in this study was higher than described in Arjmand et al. where a decrease in weight of 3% of the oxygen carrier was observed during reduction with methane at 925 °C [21]. Chuang et al. compared CuO based alumina samples made by mechanical mixing, wet-impregnation and co-precipitation. Presence of a surface layer and CuO agglomerates inside the porous support on samples made by mechanical mixing and wet-impregnation led to a low CO_2 yield [22]. A lower CO_2 yield can be correlated with a lower efficiency of the oxygen carrier.

3.4. Influence of impregnation on looping efficiency

The looping efficiency was determined from the mass of granulates before and after reduction. This corresponds to the amount of oxygen that is interchanged during the reactions. Fig. 7 represents

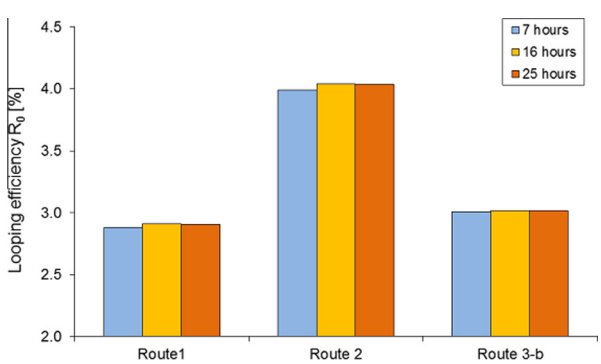

Fig. 7. Looping efficiencies.

the looping efficiency of the three different samples after 7, 16 and 25 h test. Sample from Route 2 showed a high looping efficiency compared to the samples from Routes 1 and 3-b. One reason will be the higher copper phase impregnation (12%) in comparison to samples from Route 1 and Route 3-b, which were incubated with 10% and 9% copper phases, respectively.

3.5. Phase analyses

Phase analyses of impregnated samples after drying, calcination and during CLC experiments were determined by X-ray diffraction. Because of the large number of patterns of granulates composed of multi-materials, it was preferred to only compare the presence of copper phases (Table 3). Patterns of support materials can be found elsewhere [12–15]. Impregnated alumina based samples after drying were composed mainly of copper nitrate hydroxide ($Cu_2(OH)_3NO_3$) because of the presence of OH groups from the alumina phase. With addition of diatomite or silica, presence of copper nitrate hydrate $Cu(NO_3)_2{\cdot}3H_2O$ was observed. CuO was the main phase after calcination, followed by copper aluminate for all samples made with different pseudo-boehmite contents. This confirms Misra and Chaklader, who mentioned the formation of $CuAl_2O_4$ at about 800 °C for γ-alumina substrates by solid-state reaction [23].

For all samples, CuO, Cu and Cu_2O phases were obtained after first reduction. Presence of Cu_2O in samples after looping experiments in reducing atmosphere confirms Chuang et al. [24]. The authors found that CuO reacts with CO to form Cu at low temperatures (250 °C). At temperatures above 700 °C, the CuO transforms first to Cu_2O and then Cu. The possible reduction of the spinel phase and its formation after further oxidation steps confirm the results of Kernke et al. [25]. Cu cations diffusion to the surface during reduction is indeed enhanced by the defects of the γ-alumina spinel structure.

Jin and Zhang mentioned that the excess of nickel reacts with alumina support during the first redox cycles, which leads to an increase of the oxygen carrier stability [26]. According to them, NiO and spinel phase $NiAl_2O_4$ lead to fast looping reactions and good regenerability. However, Ni from the spinel phase cannot be reduced completely [27]. In contrast with the developed bed materials from this study, $CuAl_2O_4$ was determined as not stable and no spinel phase was observed after 20 min of reduction [27]. Because of CuO reducing to Cu_2O and of the incomplete conversion observed by the presence of CuO after reducing atmosphere during looping experiments, it is concluded that the use of copper oxide leads to lower efficiency than expected.

3.6. Conversion

Oxidation from CO to CO_2 at 850 °C over time was verified with mass spectroscopy on three selected supports (Figs. 8 and 9). The first support was composed of 48 vol.% clay and was sintered at

Table 3
Main copper phases present in dried, calcined samples and after oxidizing and reducing atmospheres during looping experiments of samples of the different routes.

	Copper phases			
	Dried	Calcined	After CLC cycling (reduction)	After CLC cycling (oxidation)
Route 1 48 vol.% clay_1100 °C	$Cu(NO_3)_2{\cdot}3H_2O$	CuO	Cu, Cu_2O, CuO	CuO
Route 2 0 vol.% diatomite	$Cu_2(OH)_3{\cdot}(NO_3)$	$CuAl_2O_4$	CuO, Cu, Cu_2O	$CuAl_2O_4$
Route 3-a 84 vol.% diatomite	$Cu(NO_3)_2{\cdot}3H_2O$	CuO, $CuAl_2O_4$	CuO, Cu, Cu_2O	CuO, $CuAl_2O_4$
Route 3-b (34 vol.% silica) 65 vol.% diatomite	$Cu(NO_3)_2{\cdot}3H_2O$, $Cu_2(OH)_3(NO_3)$	CuO	CuO, Cu, Cu_2O	CuO

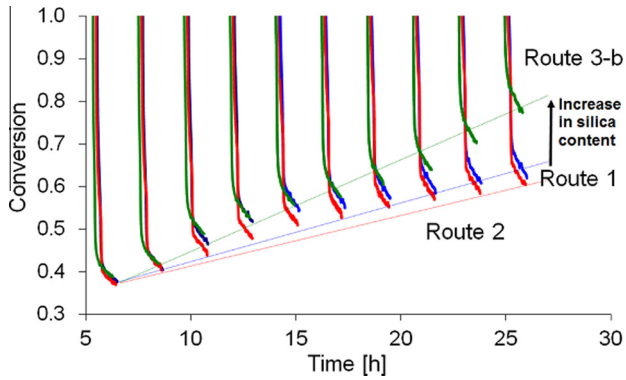

Fig. 8. Mass spectroscopy determination on three selected samples.

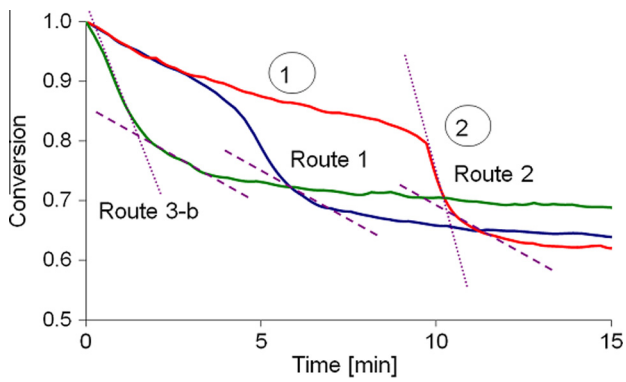

Fig. 9. Normalized mass spectroscopy's enlargement of one cycle.

1100 °C, the second one was composed of γ-alumina and the third one of alumina, 65 vol.% diatomite and 34 vol.% silica. Conversion of sample from Route 3-a was not reported in this article because of its brittleness. It was however previously tested during a shorter test [28]. It is worthwhile to note that previous reductions were applied but are not shown because the system requires few cycles to stabilize. The first slope was associated with the oxidation of CO caused by the transformation from CuO to Cu_2O of the oxygen carrier, while the second slope was associated with the transformation from Cu_2O to Cu. Conversion decreased with time, which shows the deactivation of the oxygen carrier over time. Interestingly, alumina sample showed a lower deactivation rate, followed by sample from Route 1. Interestingly, deactivation increases with increase in silica content.

Mass spectroscopy results after about 20 h were enlarged and normalized to compare the reactions (Fig. 9). As mentioned before, the first slope corresponds to the formation of Cu_2O Eq. (4). Interestingly, sample from Route 3-b, composed of the highest silica content, has the fastest and shortest reaction, while sample from Route 2, composed of alumina has the slowest. This can be explained by previous decomposition of $CuAl_2O_4$ Eq. (3) to CuO before the formation of Cu_2O Eq. (4). The second slope corresponds to the transformation from Cu_2O to Cu Eq. (5).

$$CuAl_2O_4 \rightarrow Al_2O_3 + CuO \tag{3}$$

$$CuO + CuO(CO) \rightarrow Cu_2O + CO_2 \tag{4}$$

$$Cu_2O(CO) \rightarrow 2Cu + CO_2 \tag{5}$$

As seen before, alumina sample leads to the highest conversion. The porosity and the specific surface area of the supports had no influence on the reactivity of the oxygen carrier. Macropore size

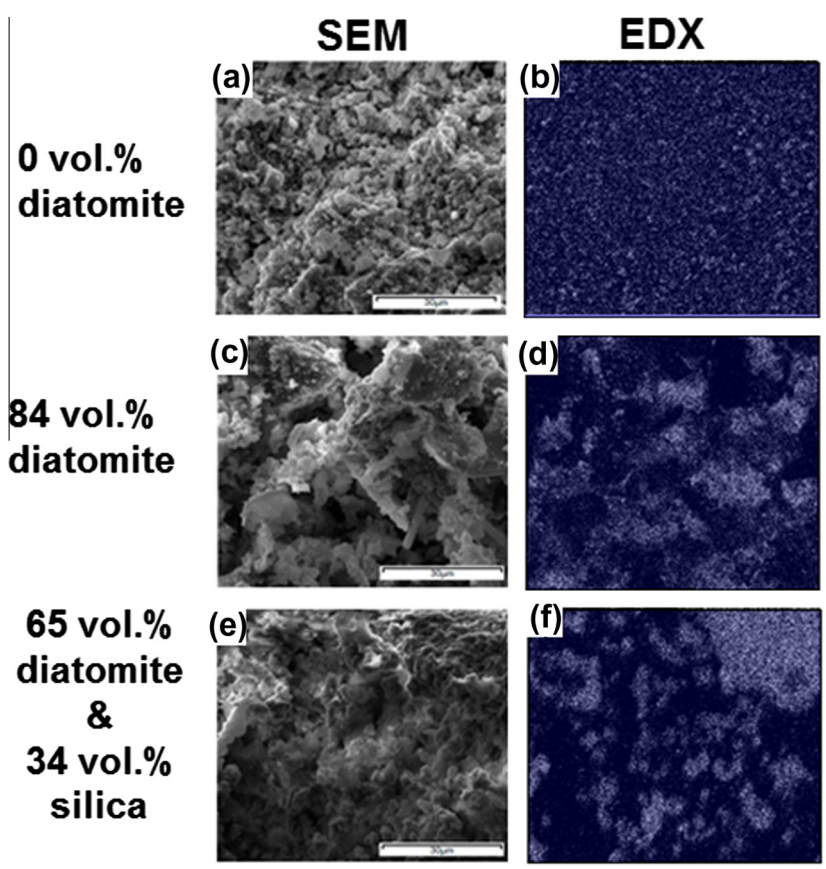

Fig. 10. Scanning electron microscopy (a, c, e) and EDX determination of copper (b, d, f) impregnated alumina sample (line 1), sample with 84 vol.% diatomite (line 2), sample with 65 vol.% diatomite and 34 vol.% silica (line 3) after looping experiments. Scale bar of 30 μm.

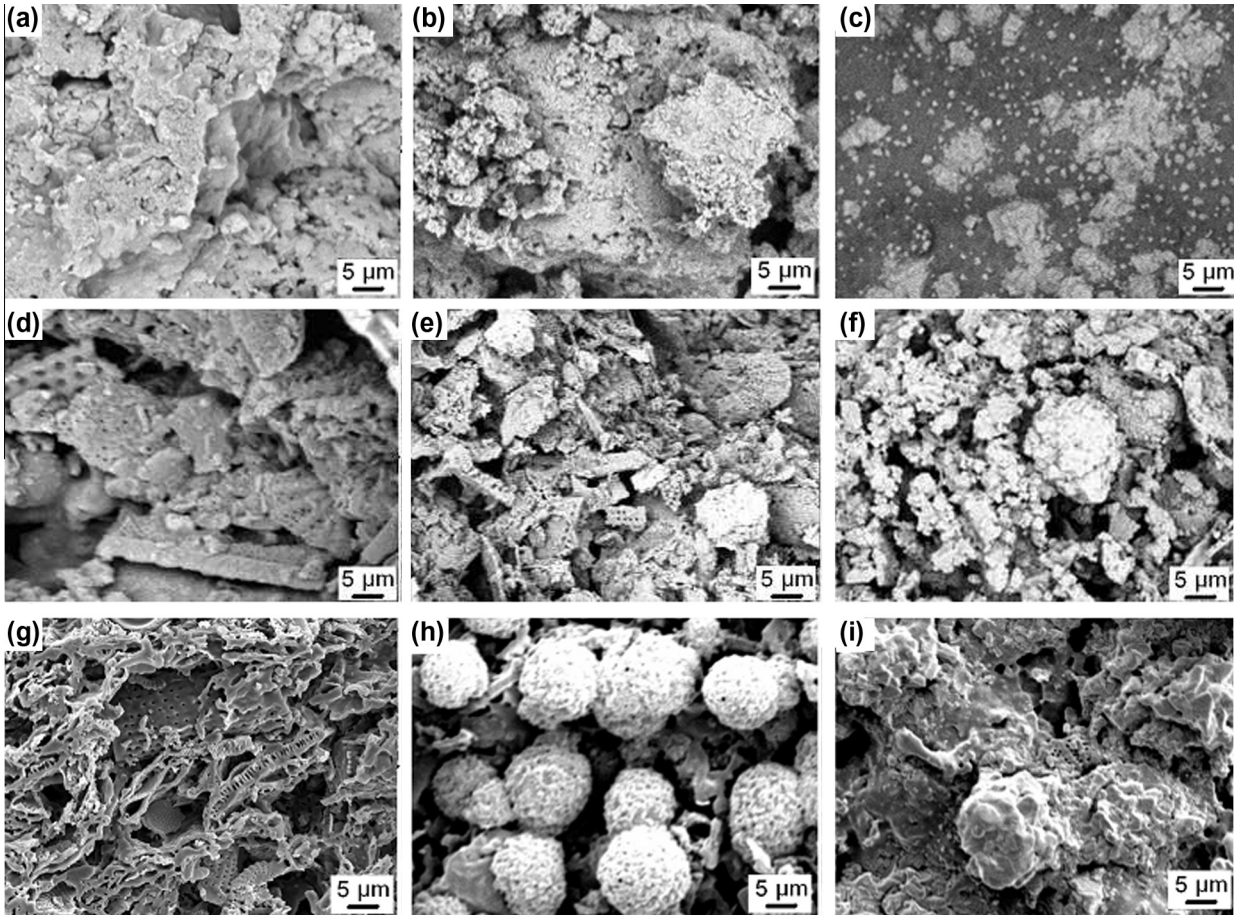

Fig. 11. Scanning electron microscopy, (a–c): alumina samples, (d–f): 84 vol.% diatomite, (g–i): 65 vol.% diatomite and 34 vol.% silica. (a, d, g) not impregnated, (b, e, h) impregnated, (c, f, i) after looping experiments.

distribution seemed however to have its importance on the reactivity. However, more important is the surface chemistry of the support.

Presence of copper element was confirmed by EDX on alumina sample (Route 2), sample with 84 vol.% diatomite (Route 3-a) and sample with 65 vol.% diatomite and 34 vol.% silica (Route 3-b) (Fig. 10, lines 1–3, respectively) after looping experiments. On the left side (Fig. 10a, c, e) corresponds to the SEM images and the right side (Fig. 10b, d, f) corresponding EDX analysis of copper distribution is present. Smaller agglomerates of copper phase were observed on alumina samples than in samples composed of diatomite with or without silica after looping experiments. This can be explained by the formation of spinel phase on the surface of the γ-Al_2O_3 substrate, which chemically bonds the copper on the substrate by reaction and building of a new chemical phase $CuAl_2O_4$. Similar results can be observed on Fig. 11, where the microstructure is compared before/after impregnation and after looping tests. Interestingly, spherical agglomerates are observed on silica based samples. It is worthwhile to mention that these samples showed high reduction of mass loss during redox cycles (Fig. 8). Reduction of redox activity by aggregation of copper has been already reported in literature [6] and is the reason why pure copper particles are not optimal for CLC applications.

3.7. Attrition resistance

Fan mentioned similar crushing strength between the support and the dry impregnated support and due to this, concluded to the importance of the support performance [1]. He recommended the use of dry impregnation for CuO and mentioned that wet impregnation will also be a suitable technique. This, despite the presence of weak bond formed between the metal oxide and the support.

In order to verify the influence of impregnation step and looping experiments on the mechanical resistance of granulates, attrition resistance after these two steps were performed on two selected materials: sample with 48 vol.% clay sintered at 1100 °C

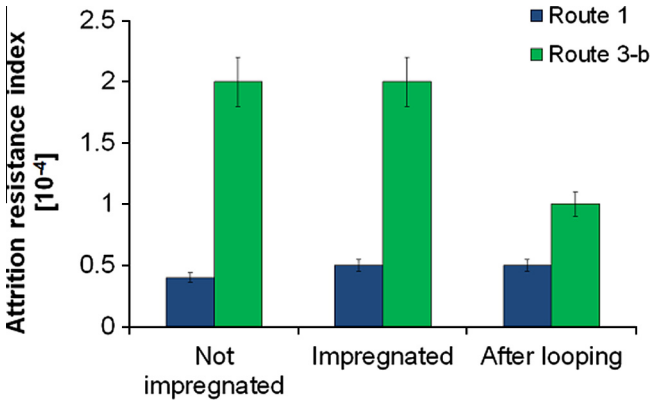

Fig. 12. Attrition resistance index of samples with 48 vol.% clay heat treated at 1100 °C (Route 1) and samples with diatomite and silica (Route 3-b), before, after impregnation and after looping experiments at 850 °C.

(Route 1) and sample with diatomite and silica, heat treated at 850 °C (Route 3-b). These two samples were selected because of their good attrition resistance. A lower attrition resistance index corresponds to a higher resistant material [12,15]. Route 1 showed indeed a higher attrition resistance than Route 3-b.

Impregnation and looping experiment at 850 °C had no effect on attrition resistance of samples from Route 1, while for the Route 3-b, higher attrition resistance (e.g. lower attrition resistance index) was observed after looping experiment because of the further sintering at 850 °C (Fig. 12). A decrease in oxidation and reduction rate after 3 cycles was observed for this sample from Route 3-b, while no change was obtained with the use of clay based sample from Route 1. This confirms that sintering during looping experiments is prejudicial for bed material efficiency. Because of its high attrition resistance, sample from Route 1 was studied for chemical looping desulfurization too with the use of Mn-basd oxides [29].

4. Conclusion

Impregnation capacity during wet impregnation process was determined as influenced mainly by the very large macropore size or specific surface area. Different copper phases were obtained according to the support, indeed use of alumina led to the formation of $CuAl_2O_4$, which was enhanced by the presence of OH groups. A decrease in specific surface area and closing of small pore volume were observed after looping experiments for Routes 2 and 3 because of the sintering of the material with further heating. Samples with diatomite showed a faster reduction, while the highest conversion was obtained with alumina sample. The slowest conversion of oxygen carrier based on alumina samples was assumed to be caused by the previous decomposition of $CuAl_2O_4$ to CuO. The main disadvantage for silica support materials is the agglomeration of copper particles during the chemical looping cycling. Wet impregnation had no effect on attrition resistance of samples from Route 1 and Route 3-b. However, an increase was observed on samples from Route 3-b after looping experiments, because of the further heating of the bed materials, which led to a sintering of the alumina/silica phase. No influence was observed on sample from Route 1 because of its higher sintering temperature (1100 °C). According to the results, composite supporting materials based on silica and alumina material are promising for future investigations.

Acknowledgments

The work was financially supported by the Competence Center Energy and Mobility (CCEM) research program of Switzerland under the project name: ARRMAT "Attrition Resistant Reactive Bed Materials in Fluidized Beds" and internal EMPA funding sources.

References

[1] L.S. Fan, Chemical Looping Systems for Fossil Energy Conversions, Wiley AlChE, NJm, 2010.
[2] W.K. Lewis, E.R. Gilliland, Production of pure carbon dioxide, US patent No. 2665972 1954.
[3] A. Lyngfelt, B. Leckner, T. Mattisson, Chem. Eng. Sci. 56 (2001) 3101–3113.
[4] C.R. Forero, P. Gayan, L.F. de Diego, A. Abad, F. Garcia-labiano, J. Adanez, Fuel Process. Technol. 90 (2009) 1471–1479.
[5] L.F. de Diego, F. García-Labiano, J. Adánez, P. Gayán, A. Abad, B. Corbella, et al., Fuel 83 (2004) 1749–1757.
[6] A. Abad, J. Adánez, F. García-Labiano, L.F. de Diego, P. Gayán, J. Celaya, Chem. Eng. Sci. 62 (2007) 533–549.
[7] T. Mattisson, A. Jardnas, A. Lyngfelt, Energy Fuels 17 (2003) 643–651.
[8] J.A. Cole, Process for separating synthesis gas into fuel cell quality hydrogen sequestration ready carbon dioxide, General Electric Co., Patent N°6667022 2003.
[9] E. Jerndal, T. Mattisson, A. Lyngfelt, Chem. Eng. Res. Des. 84 (2006) 795–806.
[10] J. Adanez, F. Garcia-Labiano, L.F. de Diego, et al., Ind. Eng. Chem. Res. 45 (2006) 2617–2625.
[11] J. Kopyscinski, Production of synthetic natural gas in a fluidized bed reactor. PhD Thesis, ETH 2010.
[12] N. van Garderen, F.J. Clemens, M. Mezzomo, C.P. Bergmann, T. Graule, Appl. Clay Sci. 52 (2011) 115–121.
[13] N. van Garderen, F.J. Clemens, D. Scharf, T. Graule, AIP Conf. Proc. 1254 (2010) 260–265.
[14] N. van Garderen, F.J. Clemens, C. Aneziris, T. Graule, Ceram. Int. 38 (2012) 5481–5492.
[15] N. van Garderen, PhD Thesis, TU Freiberg, Germany, 2013.
[16] E.P. Barrett, L.G. Joyner, P.P. Halenda, J. Am. Soc. 73 (1951) 373–380.
[17] J. Adanez, A. Abad, F. Garcia-Labiano, P. Gayan, L.F. de Diego, Prog. Energy Combust. Sci. 38 (2012) 215–282.
[18] N. van Garderen, F.J. Clemens, J. Kaufmann, M. Urbanek, M. Binkowski, T. Graule, C. Aneziris, Microporous Mesoporous Mater. 151 (2011) 255–263.
[19] N. van Garderen, T. Graule, C.G. Aneziris, F.J. Clemens, Microporous Mesoporous Mater. 171 (2013) 215–227.
[20] K. Bourikas, C. Kordulis, A. Lycourghiotis, Catal. Rev. 48 (2006) 363–444.
[21] M. Arjmand, Energy Fuels 25 (2011) 5493–5502.
[22] S.Y. Chuang, J.S. Dennsi, A.N. Hayhurst, S.A. Scott, Combust. Flame 154 (2008) 109–121.
[23] S.K. Misra, A.C.D. Chaklader, J. Am. Ceram. Soc. 46 (46) (1963) 509.
[24] S.Y. Chuang, J.S. Dennis, A.N. Hayhurst, S.A. Scott, Proc. Combust. Inst. 32 (2009) 2633–2640.
[25] R. Kernke, P. Hug, A. Reller, H.R. Ostwald, J. Therm. Anal. 38 (1992) 611–618.
[26] H. Jin, X. Zhang, in: L. Zheng (Ed.), Overview of Oxy-Fuel Combustion Technology for Carbon Dioxide (CO_2) Capture in Oxy-Fuel Combustion for Power Generation and Carbon Dioxide (CO_2) Capture, Woodheads Publishing Series in Energy, Cambridge, UK, 2011.
[27] H. Jin, T. Okamoto, M. Ishida, Ind. Eng. Chem. Res. 38 (1999) 126–132.
[28] N. van Garderen, F.J. Clemens, T. Graule, Fuel 119 (2014) 323–327.
[29] C.F.J. König, M. Nachtegaal, M. Seemann, F. Clemens, N. van Garderen, S.M.A. Biollaz, T.J. Schildhauer, Appl. Energy 113 (2014) 1895–1901.